Direct Degradation of Methylene Blue by Unactivated Peroxymonosulfate: Reaction Parameters, Kinetics, and Mechanism

Xu Zuo
second military medical university
Jianxin Nie
Fuda university
Beier Jiang
Second military medical university
Aijun Jiang
second military medical university
Shiyang Zou (zoushiyang@smmu.edu.cn)
Second Military Medical University Naval Medical Cental of PLA, Research center of water treatment and desalination
Junrong Wu
Second military medical university
Bingquan Ding
second military medical university
Xue hui Wang
second military medical unversity
Yang Liu
second military medical university

Research Article

Keywords: Peroxymonosulfate, Methylene blue, Nonradical degradation, Reaction kinetics

Posted Date: January 18th, 2022

DOI: https://doi.org/10.21203/rs.3.rs-1047490/v1

Direct degradation of methylene blue by unactivated peroxymonosulfate: Reaction parameters, kinetics, and mechanism

Xu Zuo [a,1], Jianxin Nie [b,1], Beier Jiang [a], Aijun Jiang [a], Shiyang Zou [a, *], Junrong Wu [a, *], Bingquan Ding [a], Xue hui Wang [a], Yang Liu [a]

[a] Naval Medical Center of PLA, Second Military Medical University, Shanghai , 200433, China
[b] Department of Environmental science and Engineering, Fudan University, Shanghai, 200433, China

Corresponding author:

Shiyang Zou(e-mail: zoushiyang@smmu.edu.cn)

Research center of Water treatment and desalination, Naval Medical Center of PLA, Second Military Medical University, Shanghai , 200433, China.

Junrong Wu(e-mail: 895720939@qq.com)

Research center of Water treatment and desalination, Naval Medical Center of PLA, Second Military Medical University, Shanghai , 200433, China.

Keywords: Peroxymonosulfate Methylene blue Nonradical degradation Reaction kinetics

Abstract: Advanced oxidation processes (AOPs) are efficient methods for water purification. However, there are few studies on direct oxidation with inactive peroxymonosulfate (PMS) to remove pollutants. In this study, methylene blue (MB) was oxidised efficiently by PMS. MB was decomposed through a non-radical pathway, as verified by the scavengers and electron paramagnetic resonance experiments. Although singlet oxygen was formed, the possibility of it degrading MB was ruled out via kinetics calculations. Therefore, the obvious conclusion was that PMS reacted directly with MB. Additionally, the operating parameters, including PMS dosage, MB dosage, temperature, and initial pH, were investigated. MB degradation followed pseudo-first-order kinetics, with rate constants ranging from 0.0082 to 0.3912 min^{-1}. The second-order rate constant ($k_{PMS,MB}$) for the reaction of MB with PMS was 0.08 $M^{-1}s^{-1}$ at pH 3–6, but $k_{PMS,MB}$ increased dramatically to 4.68 $M^{-1}s^{-1}$ with increasing solution pH. Chloride in the PMS/MB system reacted with PMS to form HClO, which was catalysed by PMS to rapidly decompose MB. Interestingly, MB is effectively mineralised by PMS in the presence of chlorine. In addition, humic acid, a common scavenger, did not inhibit MB degradation. In an alkaline environment, the removal rate of TOC reached 16%, but PMS caused almost no mineralisation of MB in an acidic environment. This study provides new insights into pollutant removal based on AOPs and an additional strategy for water purification.

1. Introduction

With the development of industry, environmental pollution has become a progressively larger concern, and emerging synthetic compounds with refractory biodegradability have become important for pollutant removal technologies. Advanced oxidation technology could play an important role in water treatment by efficiently destroying various kinds of pollutants, such as aromatic ring substances and azo dyes, among others. However, the mechanisms underlying pollutant degradation have not been fully elucidated (Chen et al., 2019a; Chen et al., 2018). Peroxymonosulfate (PMS), peroxydisulfate (PDS), and hydrogen peroxide (H_2O_2) are often used to generate strong oxidative species, and many methods have been developed to activate these oxidants, including the use of transition metals (Zhou et al., 2020a), UV light (He at al., 2014), a base (Qi et al., 2016), heat (Tan et al., 2015), microwaves (Monteagudo et al., 2018), carbon-based materials (Wang et al., 2020), inorganic ions (Yang et al., 2018), and organic materials (Ahamd et al., 2013). Although the activation methods are conducive to the removal of target pollutants, the energy required and heavy metals leached from catalysts increase the costs and cause secondary pollution. Furthermore, degradation efficiency is unsatisfactory because the radicals generated have poor selectivity for target pollutants when other impurities exist in the system (Long et al., 2021; Huang et al., 2019).

Due to their differences from the adjacent O–O structure, PDS, PMS, and H_2O_2 have redox potential (E^0) values of 2.01, 1.82, and 1.78 V, respectively (Qi at al., 2017; Ding et al., 2017). Furthermore, the asymmetric structure of PMS makes it unstable. In comparison with HClO (1.48 V), the redox potential of PMS enables it to thermodynamically oxidize pollutants directly. Zhou et al. (2020b) reported that PMS could degrade tetracyclines effectively in the presence of radical scavengers (methanol and tert-butyl alcohol) and a singlet oxygen scavenger (sodium azide). Ding et al. (2017) found that PDS could directly decolourize methylene blue (MB). However, the unactivated PDS could damage the structure of MB, but not rhodamine B (Yang et al., 2021a). The degradation of several sulphonamides by non-activated PMS has been compared, and aniline and dimethylisoxazole ring moieties rich in electrons were inferred to be the reactive sites (Ji et al., 2018). Recently, Yang et al. (2021b) found that oxidation by PMS was responsible for trimethoprim degradation in the trimethoprim/PMS direct system, despite the existence of singlet oxygen. The oxidation rate of chlorophenols for PMS alone was shown to increase with increased solution pH, which was attributed to the difference in degree of dissociation among several chlorophenols (Li et al., 2019). As an oxidant, PMS directly participates in the oxidation of pollutants. However, the reaction kinetics, related mechanisms, and influence of reaction parameters (PMS dosage, pollutant concentration, solution pH, temperature, and water

matrix) in the PMS oxidation system have not been studied systematically due to the complexity of the reaction environment. For example, with the exception that p-benzoquinone, a PMS oxidation by-product, activates PMS (Zhou et al., 2017), the reaction mechanisms between PMS and other pollutants have not been clarified. Moreover, research on the effects of environmental parameters on the degradation of various pollutants by PMS remains highly insufficient.

MB, a type of cationic dye and redox indicator, is used widely in the textile and dyeing industries, and for pharmaceutical processes. MB wastewater has a deep blue colour and dies not readily biodegrade. Based on previous studies, this work used MB as a model pollutant to study the reaction mechanism, kinetics, and reaction parameters in the MB/PMS system. The study aimed to provide more information about direct oxidation of pollutants by PMS, which has been overlooked in previous research.

2. Materials and methods

2.1. Chemicals and reagents

The chemicals used in this study were of analytical grade and used as received without further purification. Detailed information about the chemicals is included in Text S1 of the Supporting Information. Each solution was prepared with ultrapure water (18 MΩ cm). Detailed information about the preparation of the humic acid stock solution is described in Text S1 in the Supporting Information.

2.2. Experimental procedures

The MB degradation experiments were conducted in 150-mL conical flasks placed on a magnetic stirrer (CJJ-2S; Jintan Instrument Factory, Changzhou, China). The reaction temperature was controlled via heating in a water bath. A certain amount of MB stock solution was added to 100 mL of ultrapure water with constant stirring, and 1 mL of MB solution was withdrawn for detection of the initial MB concentration. Then, a predetermined volume of PMS stock solution was injected into the mixture to initiate MB degradation. At regular intervals, 1 mL of the mixture was sampled for detection within 1 minute. The solution pH was adjusted to the desired value with 0.1 M NaOH and H_2SO_4. A series of MB degradation experiments was evaluated under varying PMS dosage (0–4.5 mM), MB dosage (5–40 mg/L), temperature (25–45°C), initial pH (3.14–10.50), Cl^- (0–100 mM), HCO_3^- (0–100 mM), and humic acid (0–10 mg/L) conditions.

To investigate the effect of different water matrices on the decomposition of MB, 100 mL of sea water (or tap water) was used as the background solution. In addition, the pseudo-first-order kinetics were analysed as follows:

$$\ln\left(\frac{C}{C_0}\right) = -k_{obs}\, t. \quad (1)$$

In this model, C and C_0 are the MB concentration at time t and the initial concentration, respectively, and k_{obs} is the pseudo-first-order kinetic rate constant (min^{-1}).

2.3. Analytical methods

An ultraviolet spectrophotometer (TU-1810; Beijing Purkinje General Instrument Co., Ltd., Beijing, China) was used to detect MB, methyl orange (MO), and malachite green (MG) concentrations, with detection wavelengths set at 664, 465, and 612 nm, respectively. N,N-dimethylaniline (NN) was detected using high-performance liquid chromatography (G4212-6007; Agilent, Santa Clara, CA, USA) with a UV detector (detection wavelength = 240 nm) and C_{18} column (size, 250 × 4.6 mm). The mobile phase consisted of water and acetonitrile (25/75, v/v). The flow rate was set at 1 mL/min, and the injection volume was 100 μL. The reaction solution pH was monitored using a PHS-3G pH meter with an E-201F composite electrode (Shanghai LEICI CHUANGYI Instrument & apparatus Co. Ltd., Shanghai, China). The mineralisation of MB under the different conditions was determined using a TOC analyzer (Sievers M9 Portable TOC Analyzer; SUEZ Water Technologies & Solutions, Feasterville-Trevose, PA, USA). Reactive oxygen species, such as sulphate radials and hydroxyl radicals, were captured by 5,5-dimethylpyrroline N-oxide (DMPO) and the singlet oxygen reacted with 2,5,5-trimethyl-1-pyrroline N-oxide (TMPO). Then, the DMPO and TMPO adducts were detected via in situ electron paramagnetic resonance (EPR) analysis (EMXplus-10/12; Bruker, Karlsruhe, Germany). The detection parameters of the EPR were as follows: modulation frequency, 100 kHz; microwave frequency, 9.066 GHz; microwave power, 0.998 mW; and scanning range: 317.989–327.989 mT.

3. Results and discussion

3.1. Reaction mechanism

PMS has a higher redox potential (1.82 V) than HClO (1.48 V) and $KMnO_4$ (1.68 V) (Feng et al., 2019). PMS can be catalysed to generate sulphate and hydroxyl radicals, which degrade pollutants efficiently; however, in these systems, direct oxidation by PMS is usually ignored. The results shown in Fig. 1a and d suggest that PMS can decolourise MB by 75% within 180 min without the addition of a catalyst. The k_{obs} value calculated was 0.0082 min^{-1}, indicating that PMS has a greater capability to degrade MB than trimethoprim oxidation by PMS ($k_{obs} = (5.13 \pm 0.07) \times 10^{-5}$ s^{-1}) (Yang et al., 2021b).

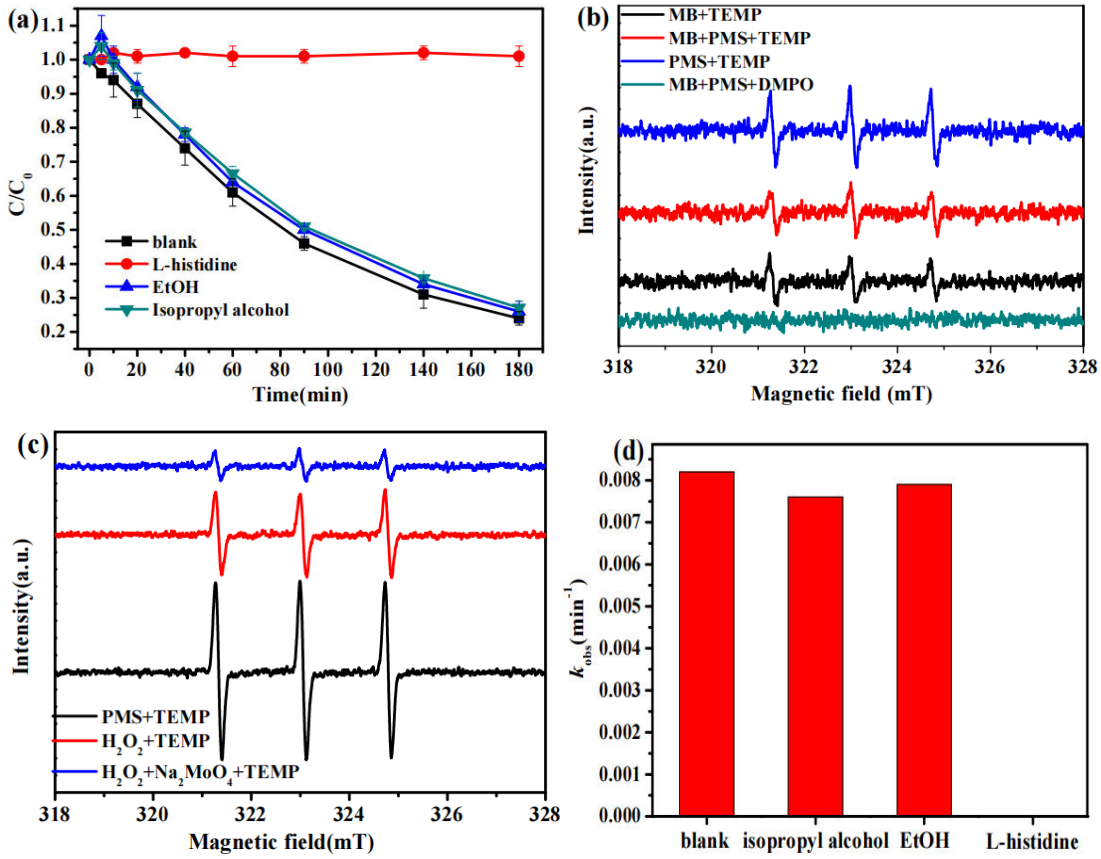

Fig. 1. (a) Degradation of methylene blue (MB) by PMS in the presence of different scavengers. (b) Electron paramagnetic resonance (EPR) spectra of TEMP-$^1O_2$ adducts formed in different cases. (c) EPR spectra of 5,5-dimethylpyrroline N-oxide (DMPO) adducts and 2,2,5-trimethyl-1-pyrroline N-oxide (TEMP) adducts in different cases. (d) k_{obs} values calculated in the presence of different scavengers. Experimental conditions: [MB] = 10 mg/L, [PMS] = 1.5 mM, [EtOH] = [isopropyl alcohol] = 150 mM, [TEMP] = [DMPO] = 100 mM, [H_2O_2] =10 mM, [Na_2MoO_4] = 1 mM, reaction temperature = 25°C, pH unadjusted.

A series of experiments were conducted to study the reactive substances and explore the degradation mechanism. Ethanol reacts with both sulphate and hydroxyl radicals with high second-order kinetic rate constants, and can be used as a scavenger, whereas isopropyl alcohol reacts rapidly with hydroxyl radicals but not with sulphate radicals (Sun et al., 2021; Sun et al., 2019). Thus, these two alcohols were employed to determine whether radicals are involved in the degradation of MB. L-histidine is usually used to capture singlet oxygen. The data in Fig. 1a and d show that the removal rate of MB was as high as 75%, and that it only dropped by 2% and 3.1% in the presence of ethanol and isopropyl alcohol, respectively. k_{obs} values declined only slightly. from 0.0082 to 0.0079 and 0.0076 min^{-1}, respectively, indicating that radicals played only a minor role in damaging MB. Furthermore, the MB degradation rate was 58% and 52.5%, and k_{obs} was 0.005 and 0.0045 min^{-1}, in the presence of 1.5 M ethanol and isopropyl alcohol, respectively (Fig. S1).

Notably, the reduction in degradation rate and k_{obs} might be attributable to the increase of solution viscosity under the high doses of alcohol, which prevented PMS and MB from diffusing and prevented decolourisation (Guan et al., 2014). On the other hand, the complete inhibition of MB removal by addition of L-histidine may be an indication of singlet oxygen in the PMS/MB system.

EPR spectroscopy was performed to confirm reactive species in the system directly. As shown in Fig. 1b, there was no signal of DMPO–SO_4 or DMPO–OH in the system, consistent with the results of the radical scavenging experiments. On the contrary, a three-peak, equal-strength signal provided evidence of singlet oxygen. It is well known that self-decomposition of PMS can generate singlet oxygen at an extremely low rate. Notably, the intensity of singlet oxygen is weak in Fig. 1c because it survived for only 4.2 μs in the H_2O and was scavenged rapidly by H_2O ($k = 2.5 \times 10^5 s^{-1}$) (Yang et al., 2018; Bohme et al., 1992). MB, an excellent photosensitised organic material (Yao et al., 2019), can produce singlet oxygen under light illumination, which was verified by the result in Fig. 1c. Yang et al. (2018) stated that L-histidine reacted directly with PMS, and that the PMS was consumed completely within a few minutes. Additionally, Liao et al. (2021) observed that the suppression of methyl parathion by PMS oxidation with addition of furfuryl alcohol was attributable to the furfury alcohol reacting with PMS. Therefore, although L-histidine captures singlet oxygen efficiently, it can be inferred that it may consume PMS in a largely spontaneously manner and thus suppress MB degradation. To verify this hypothesis, singlet oxygen was generated in situ according to a previous report (Bohme et al., 1992), and the degradation of MB by singlet oxygen in the H_2O_2/Na_2MoO_4/MB system was assessed. The generation rate of singlet oxygen was as high as ~30 μM s^{-1} at pH 9.30, comparable to the rate of MB under light (Bohme et al., 1992). Figure 1c shows that the characteristic signal of singlet oxygen in the H_2O_2/Na_2MoO_4 system was stronger than that of PMS alone, in agreement with prior research (Bohme et al., 1992). Nevertheless, the removal rate of MB in Fig. S2, even at a high concentration of singlet oxygen, was only 13%, and the k_{obs} value was about 1.06×10^{-3} min^{-1}. This result indicated that singlet oxygen was not responsible for the MB removal. Moreover, Lu et al. (2021) found the same interesting phenomenon: although singlet oxygen existed in the system, it barely degraded isoproturon.

To further evaluate the effect of singlet oxygen on the degradation of MB, the dynamic calculation method was employed. The second-order rate constant of PMS self-decomposition is $k_5 = (7.32 \pm 0.43) \times 10^{-3} M^{-1} s^{-1}$, as listed in a previous paper (Yang et al., 2021b). The reaction equations follow:

$$^1O_2 + H_2O \rightarrow O_2 + H_2O \qquad k_1 = 2.5 \times 10^5\ s^{-1} \qquad (2)$$

$^1O_2 + MB \rightarrow$ byproducts k_2 (3)

$PMS + MB \rightarrow$ byproducts + $SO_4^{2-} + H^+$ k_3 (4)

$H_2O_2 + MB \rightarrow$ byproducts + H_2O k_4 (5)

$HSO_5^- + SO_5^{2-} \rightarrow {}^1O_2 + 2SO_4^{2-} + H^+$ k_5 (6)

In the H_2O_2/Na_2MoO_4/MB system, k'_{obs} was calculated to be 1.06×10^{-3} $min^{-1} = 1.77 \times 10^{-5} s^{-1}$. In Eq. (5), $k_4 \approx 0$ because H_2O_2 could not decompose MB (discussed below). In the other systems, $[^1O_2]_{SS}$ represents the steady state concentration of $^1O_2$, and R = 35.2×10^{-6} M s^{-1} was inferred to be the generation rate of $^1O_2$ (Bohme et al., 1992). Assuming that the generation and consumption rates of singlet oxygen were equal during the reaction process, k_2 and $[^1O_2]_{SS}$ could be calculated by the following equations:

$$k'_{obs} = k_2 [^1O_2]_{ss'} + k_4 [H_2O_2] \approx k_2 [^1O_2]_{ss}$$

$$R = (k_1 + k_2) [^1O_2]_{ss}$$

As calculated above, $k_2 = 1.26 \times 10^5$ $M^{-1}s^{-1}$ and $[^1O_2]_{ss} = 1.4 \times 10^{-10}$ M. These are similar to the values reported by Yang et al. (2018). Therefore, the second-order reaction rate constant of $^1O_2$ reacting with MB was lower than the rate constant of $^1O_2$ reacting with H_2O.

The maximum degradation rate of MB by $^1O_2$ in the PMS/MB system was calculated as follows:

$$k_5[PMS]^2 = (k_2[MB] + k_1)[^1O_2]_{ss}$$

$$d[MB]/dt = k_2 [MB] \times k_5[PMS]^2/(k_2[MB]+k_1)$$

$f = k_2[MB]/(k_1 + k_2 [MB])$, where f represents the fraction of $^1O_2$ reacting with MB (Yang et al., 2018).

Therefore, the calculated removal rate of MB was only 2.6×10^{-13} M s^{-1}; however, in this experiment, the measured value was 2.2×10^{-9} M s^{-1}. Moreover, f < 0.1% was extremely low, implying that $^1O_2$ barely contributed to MB degradation. The above results suggest that MB degradation did not depend on $^1O_2$, because of the low second-order rate reaction constant, but rather on direct oxidation by PMS through a non-radical pathway.

3.2 Effect of reaction parameters on MB degradation

3.2.1 PMS dosage

The correlation between PMS and pollutant degradation could be obtained by adjusting the PMS dosage. As shown in Fig. 2a, the removal rates of MB with increasing PMS concentration (from 0 to 0.75, 1.5, 3, and 4.5 mM) were improved to 1%, 56%, 85% and 92%, respectively. The reaction of PMS and MB was first order with the MB concentration. As presented in Fig. 2b, the k_{obs} of MB was positively proportional to the PMS concentration and the

correlation was k_{obs} = 0.0833 [PMS] (s^{-1}), implying that MB degradation was also first order with respect to PMS dosage. Furthermore, the second-order reaction rate constant of MB and PMS was estimated to be 0.0833 $M^{-1}s^{-1}$, which was much lower than the rate constant of PMS reacting with sulfamethoxazole (k_{obs} = 0.23 $M^{-1}s^{-1}$), but higher than the rate constant of PMS with trimethoprim (k_{obs} = 0.043 $M^{-1}s^{-1}$) (Ji et al., 2018; Yang et al., 2021b). This difference may be associated with the structure of the different pollutants. Ji et al. (2018) deduced that aniline and the dimethylisoxazole moiety within sulfisoxazole are the main reactive sites. This suggests that PMS selectively oxidises pollutants with electron-rich moieties because of its weak oxidative capacity.

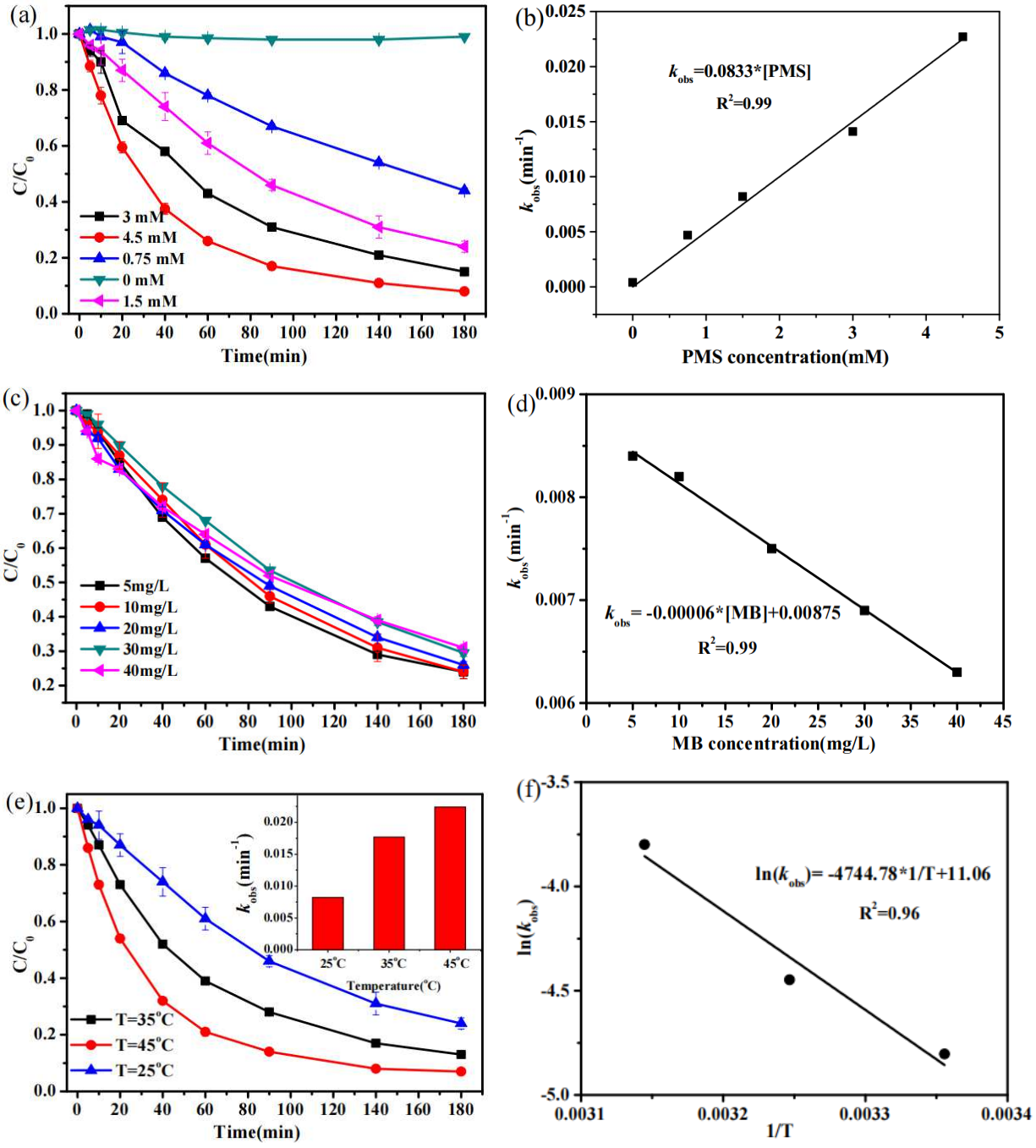

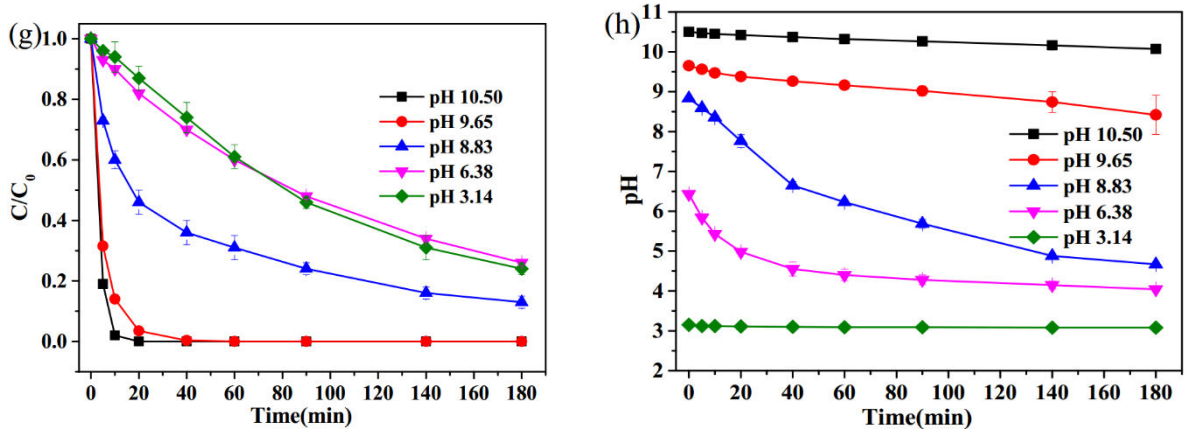

Fig. 2. Effect of (a) PMS dosage, (c) MB dosage, (e) reaction temperature, and (g) initial pH on the direct degradation by PMS, and fitting curve for the (b) PMS concentration, (d) MB concentration versus k_{obs}, and (f) ln(k_{obs}) versus 1/T. (h) Variation of solution pH during the reaction process.

3.2.2 MB dosage

To understand the potential PMS oxidation ability of this system, decomposition of different MB concentrations by PMS was performed. k_{obs} decreased gradually from 0.0082 to 0.0063 min^{-1} with MB concentration change from 5 to 40 mg/L (Fig. 2c). The plot of k_{obs} versus MB dosage obtained via linear regression analysis revealed an equation of $k_{obs} = -0.00006$ [MB] + 0.0087 (min^{-1}) (Fig. 2d). The relationship $G = (C_0 - C_{180})$ V/([PMS]V) (Text S2) was used to depict the amount of MB degraded (mg) per mmol PMS. The calculated G values were 5.1, 5.0, 4.87, 4.67, and 4.60 mg/mmol with an increase of MB from 5 to 40 mg/L. Greater MB input resulted in a reduction of PMS oxidation efficiency, possibly because of the extra consumption of PMS by MB by-products.

3.2.3 Reaction temperature

Temperature played an important role in the reaction process, and high temperature generally increased the reaction rate. The MB removal rate increased with reaction temperature (25, 35, 45°C), and the k_{obs} values were 0.0082, 0.0177, and 0.0224 min^{-1}, respectively. The removal rates were in line with k_{obs} (Fig. 2e). As shown in Fig. 2f, the activation energy was calculated based on the Arrhenius equation ($\ln k_{obs} = \ln A - E_a/RT$). The obtained E_a was approximately 43 kJ/mol, which was higher than the values (30 and 32 kJ/mol) of phenol degradation achieved by PMS activated by cobalt-functionalised activated carbon, but lower than the value (62.3 kJ/mol) in the PMS/sulfuron-methyl/chloride system (Espinosa et al., 2019; Javier et al., 2018). Peng et al. (2018) reported that the E_a in the PMS/norfloxacin system was approximately 40.3 kJ/mol. The above results implied that the degradation of MB by PMS was an endothermic reaction process, which could reduce the energy barrier for reaction of PMS with MB. Although catalysts are usually used to reduce the activation energy, the E_a value

obtained in this experiment suggests the potential for direct oxidation of MB by PMS.

3.2.4 Initial pH

The species of PMS and MB were influenced by the pH of the system according to protonation and deprotonation processes, and these PMS and MB species could affect the reaction process. Therefore, the degradation of MB was investigated in solutions with various pH. As shown in Fig. 2g, an alkaline environment was beneficial for MB degradation by PMS. The degradation of MB showed higher removal rates (Fig. 2g) and k_{obs} values with increasing pH (Fig. S3). Furthermore, the pH of the solution gradually declined due to the release of H^+ during the PMS oxidation process (Fig. 2h) (Qi et al., 2016). Shimizu et al. (2007) reported that MB is unstable and easily decolourised at pH > 10. The adjacent structure of PMS causes it to be activated easily to decolourise MB at high pH (Yang et al., 2015). Kinetics analysis was conducted using the equations below:

$$HSO_5^- + MB \rightarrow \text{byproducts} \qquad k_6 \qquad (7)$$

$$SO_5^{2-} + MB \rightarrow \text{byproducts} \qquad k_7 \qquad (8)$$

PMS had three species ($pK_{a1} < 0$, $pK_{a2} = 9.4$). In this experiment, pH values ranging from 3.14–10.50 were employed. As a cationic dye, MB had only one species, while the PMS species varied with solution pH. The result follows:

$[PMS]_{total} = \alpha_6[PMS]_0 + \alpha_7[PMS]_0 + \alpha_8[PMS]_0$ (α_6 and α_7, α_8 indicate the percentages of HSO_5^-, SO_5^{2-}, and H_2SO_5 under different pH)

$\alpha_6 = [H^+]/([H^+] + K_{a2})$

$\alpha_7 = K_{a2}/([H^+] + K_{a2})$

$\alpha_8 \approx 0$

The reaction rate of MB with PMS can be described by the following equation:

$d[MB]/dt = \sum k_i\alpha_i[PMS]_0[MB]_0$ (i = 6, 7, k_i represents the corresponding reaction rate)

$= (k_6\,\alpha_6 + k_7\,\alpha_7)[PMS]_0[MB]_0 = k_{PMS,MB}\,[PMS]_0[MB]_0$

$k_{PMS,MB} = k_6\,\alpha_6 + k_7\,\alpha_7$

As illustrated in Table 1, k_6 was estimated as 0.0865 $M^{-1}s^{-1}$, which was close to 0.0833 $M^{-1}s^{-1}$, suggesting that HSO_5^- was the main species of PMS under low solution pH (pH < 7). However, as the pH value of the solution increased, SO_5^{2-} became the main species, and k_7 increased dramatically (10-fold) when the solution became alkaline. Liao et al. (2021) found that the transformation of methyl parathion by PMS was also complex under different pH values. This change was attributed to three aspects: the high reactivity and electrostatic attraction

between SO_5^{2-} and MB, easy decolourisation of MB under an alkaline environment (Shimizu et al., 2007), and enhanced alkalinity promoting activation of PMS for generation of $^1O_2$ and superoxide anion radicals (Qi et al., 2016).

Table 1 The reaction kinetics parameters at different initial pH

Initial pH	k_{obs} (min^{-1})	HSO_5^- percentage	k_6 ($M^{-1}s^{-1}$)	k_7 ($M^{-1}s^{-1}$)
3.14	0.0082	99.99%	0.091	—[a]
6.38	0.0074	99.90%	0.082	—[a]
8.83	0.011	78.79%	0.0865[b]	0.254
9.65	0.1406	34.94%	0.0865[b]	2.354
10.50	0.3912	7.36%	0.0865[b]	4.68

a: The percentage of SO_5^{2-} was below 0.1% and the contribution of k_{obs} was ignored.

b: The value was obtained via (0.091 + 0.082)/2. The difference of k_6 between pH 3.14 and 6.38 was about 10%.

3.3 Effect of coexisting ions and humic acid

The chloride content in a natural body of water or wastewater treatment plant ranges from tens to hundreds of mg/L, and the drainage usually amounts to thousands of mg/L. In particular, higher concentrations of chloride are released by the metal smelting industry. Chloride can be oxidised by strong oxidants to generate HClO, which is used widely as an oxidant and bleaching agent, via the loss of an electron. As depicted in Fig. 3a, chloride accelerated degradation of MB, and the promotion effect increased with increased chloride concentration. However, the addition of NH_4^+ inhibited the degradation of MB in the presence of chlorine (Fig. S4). NH_4^+ can be deprotonated into NH_3, which can react with HClO to induce the formation of chloramines (Deborde et al., 2008). The k_{obs} in the chloride system with NH_4^+ addition was obviously lower than the value in the system without NH_4^+, suggesting that Cl^- competes with MB for PMS (Fig. 3b) (Eqs. 9–11). Bromide can also be oxidised by PMS to generate HBrO, which was shown to accelerate the oxidation of tetrabromobisphenol S (Xu at al., 2021). Moreover, although PMS was consumed to generate HClO, the residual portion could still oxidise the majority of the MB when HClO was scavenged by NH_3, and the k_{obs} dropped only slightly in comparison to the value in the PMS/MB system (Fig. 3b). This result indicated that the degradation of MB by PMS in the presence of chlorine was relatively low, and that the main factor leading to the degradation of MB may be the catalysis of PMS on chlorine. Ding et al. (2021) found that PMS did not react with chlorine but could be catalysed by chlorine to react with

acetaminophen. Therefore, the high reaction rate in the presence of chloride might occur through three steps: chloride reacting with PMS to generate HClO as the rate-limiting reaction (a determined step); decomposition of MB by HClO catalysed by PMS (main step); direct degradation of MB by PMS (minor step).

S(IV) can also scavenge radicals. Therefore, the effect of a reducing agent ($NaHSO_3$) on MB degradation by PMS was investigated. As shown in Fig. S5, MB decolourisation was almost inhibited with PMS alone. Nevertheless, with the addition of 10 and 50 mM chloride, the MB removal rate increased up to 32% and 76%, respectively. Connick et al. (1995) reported that PMS reacted with HSO_3^- in two ways: (1) via the formation of sulphate radicals, with an extremely slow reaction rate (Eq. (12)); and (2) via the production of a sulphate ion and proton with a fast reaction rate in comparison to (1) (Eq. (13)). PMS was consumed by HSO_3^-, so the removal rate of MB diminished significantly. The chloride ion was able to react with the residual PMS (about 0.5 mM PMS) to form HClO, and the HClO was catalysed by PMS to accelerate the oxidation of MB. Hence, when a reducing agent was present in the PMS system, the diminished removal of organic matter could be compensated by the addition of chloride.

$$HSO_5^- + 2Cl^- + 2H^+ \rightarrow HSO_4^- + Cl_2 + H_2O \qquad k = (2.06 \pm 0.03) \times 10^{-3} M^{-1}s^{-1} \qquad (9)$$

$$HSO_5^- + Cl^- \rightarrow SO_4^{2-} + HClO \qquad (10)$$

$$Cl_2 + H_2O \rightarrow HClO + HCl \qquad (11)$$

$$HSO_5^- + HSO_3^- \rightarrow SO_4^{2-} + SO_3^{\cdot-} + H_2O \qquad k = (0.05–0.28)\ M^{-1}s^{-1} \qquad (12)$$

$$HSO_5^- + HSO_3^- \rightarrow 2SO_4^{2-} + 2H^+ \qquad (13)$$

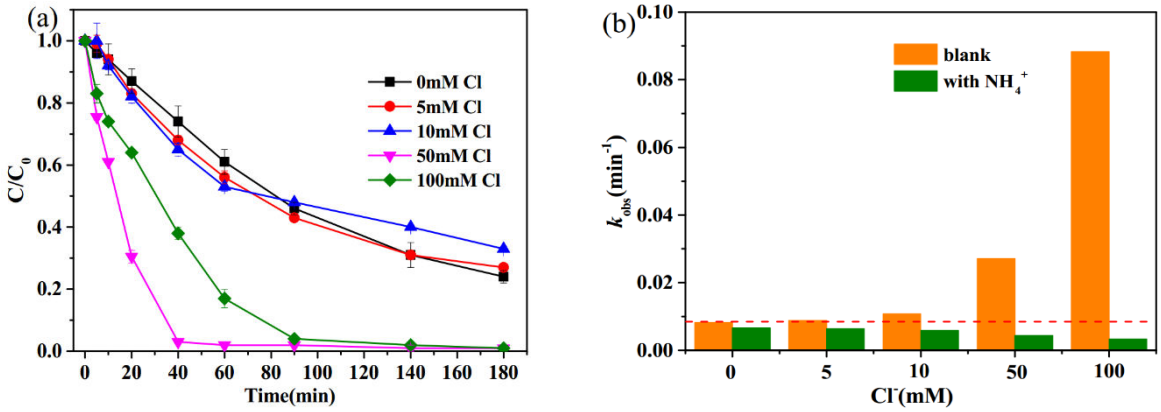

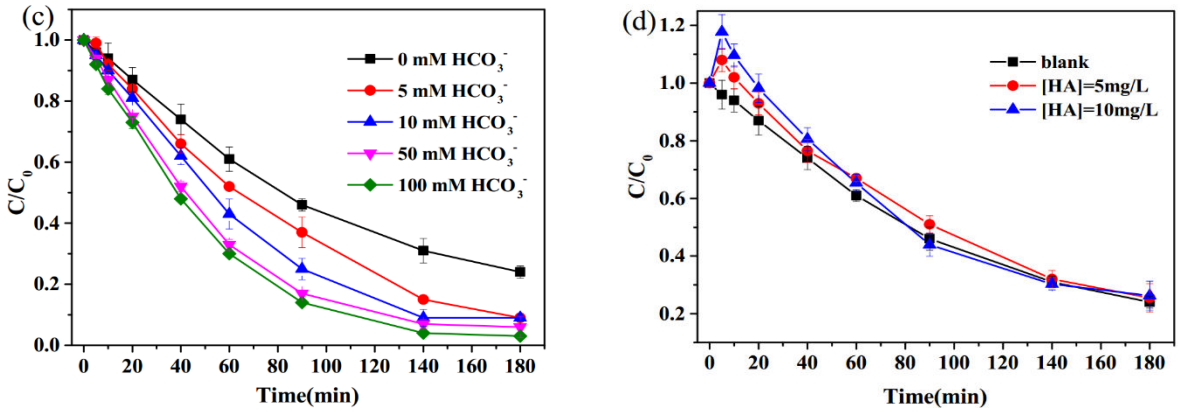

Fig. 3. Effect of (a) chloride, (c) bicarbonate, and (d) humic acid on MB degradation by PMS, and (b) k_{obs} of MB degradation in the presence of chloride and NH_4^+. Experimental conditions: [MB] = 10 mg/L, [PMS] = 1.5 mM, [NH_4^+] = 150 mM, reaction temperature = 25°C, pH unadjusted.

Bicarbonate is a common substance in surface bodies of water. Therefore, it is essential to investigate the effect of bicarbonate on the degradation of MB from the viewpoint of practical application (Song et al., 2019; Chen et al., 2019b). As illustrated in Fig. 3c, bicarbonate improved the removal rate of MB by PMS. The reaction rate was also accelerated from 0.0082 to 0.021 min^{-1} (Fig. S4). The addition of bicarbonate increased the solution pH (higher than 8.0 during the reaction process), and the alkaline environment was beneficial for the decomposition of MB. Furthermore, Yang et al. (2018) found that PMS could be catalysed by bicarbonate to form singlet oxygen. The effect of bicarbonate on MB removal was consistent with the results showing that the degradation of the azo dye Acid Orange 7 by PMS oxidation was activated by bicarbonate (Yang et al., 2010).

The dissolved organic matter in a natural body of water is composed of a carbon skeleton with abundant oxygen-containing functional groups at the surface, and the effect of humic acid on MB degradation can be ignored (Fig. 3d). For removal rates of 76%, 74.5%, and 77%, the k_{obs} values of MB degradation were 0.0082, 0.0081, and 0.0087 min^{-1}, respectively (Fig. S4). Humic acid reacted with sulphate radicals and hydroxyl radicals with second-order rate constants of 2.35×10^7 and 3×10^8 $M^{-1}s^{-1}$, respectively (Xie et al., 2015; Pang et al., 2018), further suggesting that the MB oxidation by PMS was a radical reaction process.

3.4 Universal degradation of other typical dyes

Different structures and physical and chemical properties can significantly affect the reaction between pollutants and oxidants. Three common dyes (MB, MO, and MG) were selected to investigate the capacity for PMS oxidation. MO is a typical azo dye, MB is a commonly used cationic dye, and MG is a type of toxic triphenylmethane dye. The k_{obs} values of MO, MB, and MG were 0.0733, 0.0082, and 0.0491 min^{-1}, respectively (Fig. 4b), and the removal rates were 89%, 76%, and 99%, respectively, indicating that PMS could decompose the

three dyes efficiently (Fig. 4a). Different from the cases of MB and MG, the NN moiety in MO is an electron-donating group and the sulfonic acid group is an electron-withdrawing group. The interaction of the two groups induced the electron clouds to be attracted to the side of the azo bond that was easily attacked by the electrophilic reagent PMS. This result agrees with previous studies (Guo et al., 2021; Chen et al., 2019c; Nie et al., 2019; Liu et al. 2015) reporting that decolourisation took precedence over degradation of the benzene ring. The NN moiety is the common sub-structure among the three dyes, and NN was degraded by more than 90% within 5 min by direct oxidation by PMS (Fig. S6). The higher reaction rate of NN compared to other parent dyes may indicate that NN was the reactive site of the three dyes. The lower reaction rates than the rate of NN might be attributable to an effect of other sub-structures on the parent dyes (Ji et al. 2018). The formation of the conjugated system in the three parent dyes prompted the rearrangement of electron clouds. However, the introduction of strong electron-withdrawing groups induced a reduction of the energy barrier and electrons could escape easily (Titov et al., 2015). Further research is needed to understand the details of the mechanism.

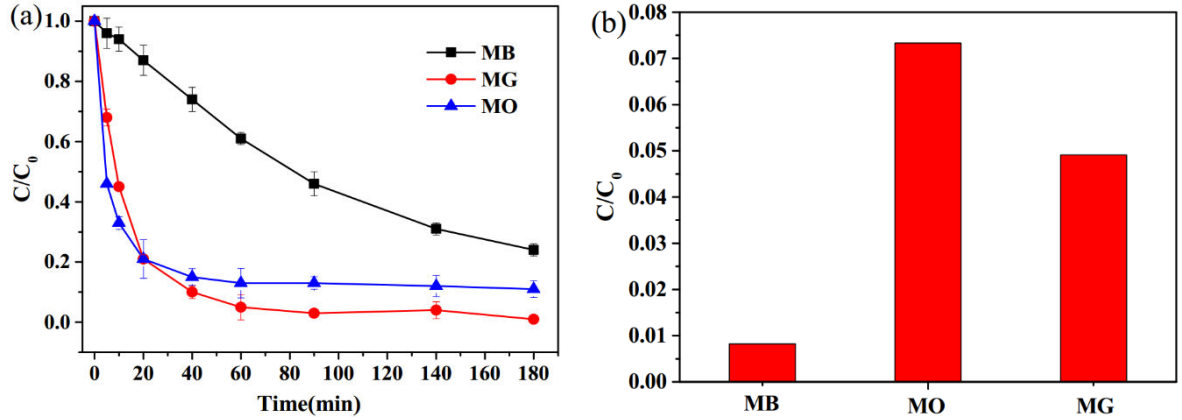

Fig. 4. (a) Direct degradation of MB, MG, and MO by PMS and (b) k_{obs} of the MB, MG, and MO degradation. Experimental conditions: [MB] = [MO] = [MG] = 10 mg/L, [PMS] = 1.5 mM, reaction temperature = 25°C, pH unadjusted.

3.5 Effect of water matrix

To understand the MB degradation performance of advanced oxidation processes (AOPs) more completely, two types of water (sea water and tap water) were employed. Sea water was collected from the South China Sea and tap water was obtained from Shanghai, China. The water quality of the two samples is described in Table S1. The MB removal and reaction rates in the above waters were better than those in ultrapure water (Fig. 5). Especially, the high chloride content of sea water promoted MB degradation. Although the two water matrices contained dissolved organic matter, which competed with MB for radicals, PMS reacted with MB directly without generating radicals. The results from the application of the two water types suggest that PMS is an efficient choice for real water

sample purification.

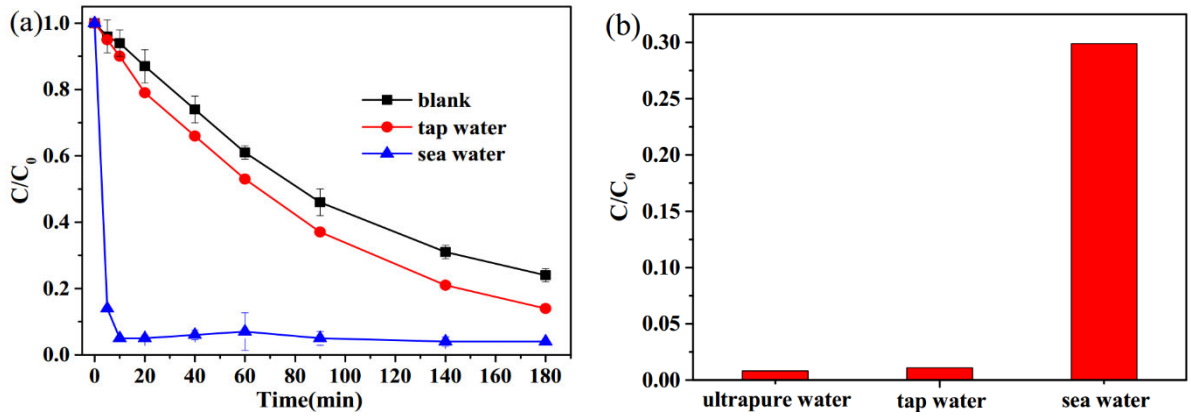

Fig. 5. (a) Effect of different water matrices on the degradation of MB by unactivated PMS. (b) k_{obs} of MB degradation under different water matrices. Experimental conditions: [MB] = 10 mg/L, [PMS] = 1.5 mM, reaction temperature = 25°C, pH unadjusted.

3.6 TOC removal in different reaction conditions

Total organic carbon (TOC) is an important indicator of the mineralising capacity of pollutants in a system. In this study, the pollutants were first decomposed into small molecular substances and then oxidised into carbon dioxide and water. The results of the TOC removal are shown in Fig. 6. The TOC removal rate was near zero at pH 3.14. However, it increased to 16% at pH 10.5. In the presence of 50 mM chloride, the TOC removal rate was 45%. These results suggest that PMS alone can barely mineralise MB and only damaged the chromogenic group of the MB. Zhou et al. (2020b) found that MB oxidation by PMS proceeded through oxygenation, demethylation, and deamination processes, but the main structure of MB remained unchanged. The TOC removal rate of AO7 by PMS alone was only 19.2%, suggesting that the mineralisation capacity in the PMS system was low (Chen et al., 2021). Under the highly alkaline environment, SO_5^{2-} was the main species of PMS, and it reacted with MB rapidly through the mineralisation process. Additionally, the formation of singlet oxygen and superoxide anion radicals via PMS self-decomposition selectively degraded pollutants with electron-rich moieties. Therefore, more recalcitrant by-products were formed in the reaction process and could barely be mineralised. In the presence of chloride, the HClO that formed had a strong capacity to oxidise the chromogenic group and further mineralise MB with catalysis by PMS. Wang et al. (2011) pointed out that the TOC removal rate of azo dyes in the Co/PMS/Cl system was lower than 5% within 450 s, indicating that chloride could improve the decolourisation ability but not the TOC removal rate. Yuan et al. (2011) reported that although the sulphate and hydroxyl radicals formed in the Co/PMS system had strong redox potential, the oxidation ability of chlorine radicals generated by the reaction of other radicals with chlorine was low in comparison to the sulphate and hydroxyl radicals. Additionally, the chlorine radicals reacted

with azo dyes or by-products to form refractory organic halogen compounds, which are difficult to mineralise. However, on the contrary, the addition of chloride enhanced the TOC removal rate in this study, which may be attributable to HClO replacing, and being catalysed by, PMS. However, with the generation of organic halogen compounds and the consumption of PMS, mineralisation gradually ceased.

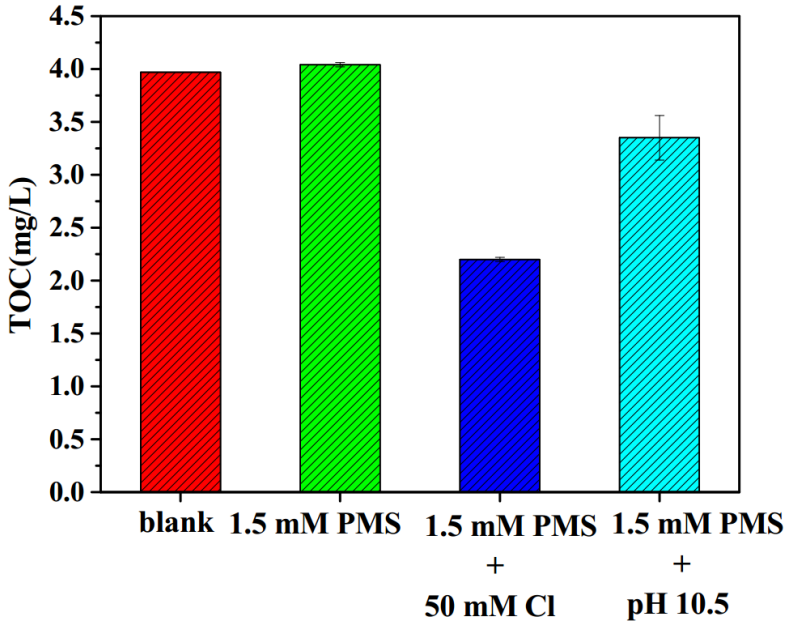

Fig. 6. Variation of TOC under different circumstances. Experimental conditions: [MB] = 10 mg/L, reaction temperature = 25°C, pH unadjusted (except where specified).

4. Conclusion

AOPs based on radicals have strong oxidation abilities, allowing the removal of a broad range of organic micropollutants. However, direct oxidation by PMS for water purification has been overlooked. The reaction mechanism, kinetics, and parameters of PMS reacting with MB found in this study can be summarized as follows:

(1) PMS reacted with MB via a non-radical pathway. Additionally, the second-order rate constant of MB reacting with singlet oxygen was estimated to be approximately 1.25×10^5 $M^{-1}s^{-1}$.

(2) The pseudo-first-order rate constant of MB transformation showed a negative linear correlation with the MB concentration and a positive linear correlation with the PMS concentration.

(3) Increasing the solution pH favoured MB degradation by PMS, which was attributed to the high reaction rate between SO_5^{2-} and MB.

(4) The addition of chloride accelerated MB transformation and mineralisation by PMS due to the formation of HClO and catalysis by PMS.

(5) In real water matrices (sea water and tap water), MB degradation was promoted. Even in water with added humic acid, MB degradation was not affected, suggesting an advantage of the PMS oxidation system.

Above all, this study aimed to provide deeper insight into AOPs based on the PMS oxidation system and thus provide an alternative solution for the treatment of environmental pollution.

Ethical approval

Not applicable.

Consent to participate

The authors all agree to participate in the paper.

Consent to publish

The authors all agree that the paper is published in the journal.

Credit author statement

Xu Zuo: Conceptualization, Investigation, Writing - original draft. **Jianxin Nie:** Writing - review & editing. **Beier Jiang:** Editing. **Aijun Jiang:** Methodology. **Shiyang Zou:** Editing & Supervision. **Junrong Wu:** Supervision. **Bingquan Ding:** Investigation. **Xuehui Wang:** Validation. **Yang Liu:** Investigation.

Funding

This work was supported by National Military Standard Research Project of China(20CH0612).

Declaration of competing interest

The authors report no declarations of interest.

Availability of data

All data generated or analyzed during this study are included in this published article.

References

Ahmad M, Teel A, Watts R (2013) Mechanism of persulfate activation by phenols. Environmental Science & Technology 47, 5864-5871.

Bohme K, Brauer H, (1992) Generation of singlet oxygen from hydrogen peroxide disproportionation catalyzed by molybdate ions. Inorganic Chemistry 31, 3468-3471.

Chen L, Zuo X, Yang S, Cai T, Ding D (2019a) Rational design and synthesis of hollow Co_3O_4@Fe_2O_3 core-shell nanostructure for the catalytic degradation of norfloxacin by coupling with peroxymonosulfate. Chemical Engineering Journal 359, 373-384.

Chen X, Oh W, Lim T (2018) Graphene- and CNTs-based carbocatalysts in persulfates activation: Material design and catalytic

420 mechanisms. Chemical Engineering Journal 354, 941-976.
421 Chen X, Yang B, Oleszczuk P, Gao Y, Yuan X, Ling W, Waigi M (2019b) Vanadium oxide activates persulfate for degradation of
422 polycyclic aromatic hydrocarbons in aqueous system. Chemical Engineering Journal 364, 79-88.
423 Chen Y, Tong Y, Liu Z, Huang L, Yuan J, Xue Y, Fang Z (2019c) Enhanced degradation of Orange II using a novel
424 UV/persulfate/sulfite system. Environmental Chemistry Letters 17(3), 1435-1439.
425 Chen Z, Wan Q, Wen G, Luo X, Xu X, Wang J, Li K, Huang T, Ma J (2021) Effect of borate buffer on organics degradation with
426 unactivated peroxymonosulfate: Influencing factors and mechanisms. Separation and Purification Technology 256, 117841.
427 Connick R, Zhang Y, Lee S, Adamic P (1995) Kinetics and mechanism of the oxidation of HSO_3^- by O_2. 1. The uncatalyzed reaction.
428 Inorganic Chemistry 34, 4543-4553.
429 Deborde M, von Gunten U (2008) Reactions of chlorine with inorganic and organic compounds during water treatment-kinetics and
430 mechanisms: a critical review. Water Research 42(1-2), 13-51.
431 Ding D, Liu C, Ji Y, Yang Q, Chen L, Jiang C, Cai T (2017) Mechanism insight of degradation of norfloxacin by magnetite
432 nanoparticles activated persulfate: Identification of radicals and degradation pathway. Chemical Engineering Journal 308,
433 330-339.
434 Ding J, Nie H, Wang S, Chen Y, Wan Y, Wang J, Xiao H, Yue S, Ma J, Xie P (2021) Transformation of acetaminophen in solution
435 containing both peroxymonosulfate and chlorine: Performance, mechanism, and disinfection by-product formation. Water
436 Research 189, 116605.
437 Espinosa J, Manickam-Periyaraman P, Bernat-Quesada F, Sivanesan S, Álvaro M, García H, Navalón S (2019) Engineering of
438 activated carbon surface to enhance the catalytic activity of supported cobalt oxide nanoparticles in peroxymonosulfate activation.
439 Applied Catalysis B: Environmental 249, 42-53.
440 Feng M, Baum J, Nesnas N, Lee Y, Huang C, Sharma V (2019) Oxidation of sulfonamide antibiotics of six-membered heterocyclic
441 moiety by Ferrate(VI): kinetics and mechanistic insight into SO_2 extrusion[J]. Environmental Science & Technology 53(5),
442 2695-2704.
443 Guan Y, Ma J, Ren Y, Liu Y, Xiao J, Lin L, Zhang C (2013) Efficient degradation of atrazine by magnetic porous copper ferrite
444 catalyzed peroxymonosulfate oxidation via the formation of hydroxyl and sulfate radicals. Water Research 47(14), 5431-5438.
445 Guo Z, Bai G, Huang B, Cai N, Guo P, Chen L (2021) Preparation and application of a novel biochar-supported red mud catalyst:
446 Active sites and catalytic mechanism. Journal of Hazardous Materials 408, 124802.
447 He X, Mzeyk S, Michael I, Fatta-Kassinos D, Dionysiou D (2014) Degradation kinetics and mechanism of beta-lactam antibiotics by
448 the activation of H_2O_2 and $Na_2S_2O_8$ under UV-254 nm irradiation. Journal of Hazardous Materials 279, 375-383.
449 Huang D, Wang T, Zhu K, Zhao S, Shi Y, Ye M, Wang C, Jia H (2019) Low-molecular-weight organic acids impede the degradation of

450 naphthol in iron oxides/persulfate system: Implications for research experiments in pure conditions. Chemosphere 225, 1-8.
451 Li C, Wang Y, Chen C, Fu X, Cui S, Lu J, Liu H, Li W (2019) Interactions between chlorophenols and peroxymonosulfate: pH
452 dependency and reaction pathways. Science of the Total Environment 664, 133-139.
453 Liao X, Cao J, Hu Y, Zhang C, Hu L (2021) Mechanism of unactivated peroxymonosulfate-induced degradation of methyl parathion:
454 Kinetics and transformation pathway. Chemosphere 284, 131332.
455 Liu X, Yang Y, Shi X, Li K (2015) Fast photocatalytic degradation of methylene blue dye using a low-power diode laser. Journal of
456 Hazardous Materials 283, 267-275.
457 Long X, Yang S, Qiu X, Ding D, Feng C, Chen R, Tan J, Wang X, Chen N, Lei Q (2021) Heterogeneous activation of
458 peroxymonosulfate for bisphenol A degradation using $CoFe_2O_4$ derived by hybrid cobalt-ion hexacyanoferrate nanoparticles.
459 Chemical Engineering Journal 404, 127052.
460 Lu J, Ji Y, Chovelon J, Lu J (2021) Fluoroquinolone antibiotics sensitized photodegradation of isoproturon. Water Research 198,
461 117136.
462 Monteagudo J, El-Taliawy H, Duran A, Caro G, Bester K (2018) Sono-activated persulfate oxidation of diclofenac: Degradation,
463 kinetics, pathway and contribution of the different radicals involved. Journal of Hazardous Materials 357, 457-465.
464 Nie M, Zhang W, Yan C, Xu W, Wu L, Ye Y, Hu Y, Dong W 2(019) Enhanced removal of organic contaminants in water by the
465 combination of peroxymonosulfate and carbonate. Science of the Total Environment 647, 734-743.
466 Javier F, Solís R, (2018) Chloride promoted oxidation of tritosulfuron by peroxymonosulfate. Chemical Engineering Journal 349,
467 728-736.
468 Ji Y, Lu J, Wang L, Jiang M, Yang Y, Yang P, Zhou L, Ferronato C, Chovelon J (2018) Non-activated peroxymonosulfate oxidation of
469 sulfonamide antibiotics in water: Kinetics, mechanisms, and implications for water treatment. Water Research 147, 82-90.
470 Pang Y, Tong Z, Tang L, Liu Y, Luo K (2018) Effect of humic acid on the degradation of methylene blue by peroxymonosulfate. Open
471 Chemistry 16(1), 401-406.
472 Peng Q, Ding Y, Zhu L, Zhang G, Tang H (2018) Fast and complete degradation of norfloxacin by using Fe/Fe_3C@NG as a
473 bifunctional catalyst for activating peroxymonosulfate. Separation and Purification Technology 202, 307-317.
474 Qi C, Liu X, Li Y, Li C, Ma J, Li X, Zhang H (2017) Enhanced degradation of organic contaminants in water by peroxydisulfate
475 coupled with bisulfate. Journal of Hazardous Materials 328, 98-107.
476 Qi C, Liu X, Ma J, Lin C, Li X, Zhang H (2016) Activation of peroxymonosulfate by base: Implications for the degradation of organic
477 pollutants. Chemosphere 151, 280-288.
478 Shimizu N, Ogino C, Dadjour M, Murata T (2007) Sonocatalytic degradation of methylene blue with TiO_2 pellets in water. Ultrasonics
479 Sonochemistry 14, 184-190.

Song W, Li J, Fu C, Wang Z, Zhang X, Yang J, William H, Gao L (2019) Kinetics and pathway of atrazine degradation by a novel method: Persulfate coupled with dithionite. Chemical Engineering Journal 373, 803-813.

Sun M, Huang W, Cheng H, Ma J, Kong, Y, Komarneni S (2019) Degradation of dye in wastewater by homogeneous Fe(VI)/$NaHSO_3$ system. Chemosphere 228, 595-601.

Sun Y, Xie H, Zhou C, Wu Y, Pu M, Niu J (2021) The role of carbonate in sulfamethoxazole degradation by peroxymonosulfate without catalyst and the generation of carbonate radicals. Journal of Hazardous Materials 398, 122827.

Tan C, Gao N, Deng Y, Li L, Deng J, Zhou S (2015) Kinetics oxidation of antipyrine in heat-activated persulfate. Desalination and Water Treatment 53(1), 263-271.

Titov E, Lysyakova L, Lomadze N, Kabashin AV, Saalfrank P, Santer S (2015) Thermal cis-to-trans isomerization of azobenzene-containing molecules enhanced by gold nanoparticles: An experimental and theoretical study. The Journal of Physical Chemistry C 119(30), 17369-17377.

Wang J, Duan X, Gao J, Shen Y, Feng X, Yu Z, Tan X, Liu S, Wang S (2020) Roles of structure defect, oxygen groups and heteroatom doping on carbon in nonradical oxidation of water contaminants. Water Research 185, 116244.

Wang Z, Yuan R, Guo Y, Xu L, Liu J (2011) Effects of chloride ions on bleaching of azo dyes by Co^{2+}/oxone regent: Kinetic analysis. Journal of Hazardous Materials 190(1-3), 1083-1087.

Xie P, Ma J, Liu W, Zhou J, Yue S, Li X, Wisner M, Fang J (2015) Removal of 2-MIB and geosmin using UV/persulfate: contribution of hydroxyl and sulfate radicals. Water Research 69, 223-233.

Xu H, Meng L, Zhao X, Chen J, Lu J, Chovelon J (2021) Accelerated oxidation of the emerging brominated flame retardant tetrabromobisphenol S by unactivated peroxymonosulfate: The role of bromine catalysis and formation of disinfection byproducts. Water Research 204, 117584.

Yang S, Wang B, Yang X, Shan L, Zhang W, Shao X, Niu R (2010) Degradation of efficiencies of azo dye Acid Orange 7 by the interaction of heat, UV and anions with common oxidants: Persulfate, Peroxymonosulfate and hydrogen peroxide. Journal of Hazardous Materials 179, 552-558.

Yang Y, Banerjee G, Brudvig G, Kim J, Pignatello J (2018) Oxidation of organic compounds in water by unactivated peroxymonosulfate. Environmental Science & Technology 52(10), 5911-5919.

Yang X, Ding X, Zhou L, Zhao Q, Ji Y, Wang X, Chovelon J, Xiu G (2021b) Direct oxidation of antibiotic trimethoprim by unactivated peroxymonosulfate via a nonradical transformation mechanism. Chemosphere 263, 128194.

Yang F, Huang Y, Fang C, Xue Y, Ai L, Liu J, Wang Z (2018) Peroxymonosulfate/base process in saline wastewater treatment: The fight between alkalinity and chloride ions. Chemosphere 199, 84-88.

Yang B, Luo Q, Li Q, Meng Y, Li L, Liu Y (2021a) Selective oxidation and direct decolorization of cationic dyes by persulfate without

activation. Water Science & Technology 83(11), 2744-2752.

Yang Y, Jiang J, Lu X, Ma J, Liu Y (2015) Production of sulfate and hydroxyl radical by reaction of ozone with peroxymonosulfate: a novel advanced oxidation process. Environmental Science & Technology 49, 7330-7339.

Yao T, Wang J, Xue Y, Yu W, Gao Q, Ferreira L, Ren K, Ji J (2019) A photodynamic antibacteria spray-coating based on the host-guest immobilization of the photosensitizer methylene blue. Journal of Materials Chemistry B 7(33), 5089-5095.

Yuan R, Ramjaun S, Wang Z, Liu J (2011) Effects of chloride ion on degradation of Acid Orange 7 by sulfate radical-based advanced oxidation process: Implications for formation of chlorinated aromatic compounds. Journal of Hazardous Materials 196, 173-179.

Zhou H, Lai L, Wan Y, He Y, Yao G, Lai B (2020a). Molybdenum disulfate(MoS_2): A versatile activation of both peroxymonosulfate and persulfate for the degradation of carbamazepine. Chemical Engineering Journal 384, 123264.

Zhou Y, Gao Y, Jian J, Shen Y, Pang S, Wang Z, Duan J, Guo Q, Guan C, Ma J (2020b) Transformation of tetracycline antibiotics during water treatment with unactivated peroxymonosulfate. Chemical Engineering Journal 379, 122378.

Zhou Y, Jiang J, Gao Y, Pang S, Yang Y, Ma J, Gu J, Li J, Wang Z, Wang L, Yuan L, Yang Y (2017) Activation of peroxymonosulfate by phenols: Important role of quinone intermediates and involvement of singlet oxygen. Water Research 125, 209-218.

Supplementary Files

This is a list of supplementary files associated with this preprint. Click to download.

- SupportingInformation20210915.doc